



3-Thiomorpholin-8-oxo-8*H*-acenaphtho [1,2-*b*] pyrrole-9-carbonitrile (**S1**) derivatives as pan-Bcl-2-inhibitors of Bcl-2, Bcl- x_L and Mcl-1 [☆]

Ting Song^{a,†}, Xiangqian Li^{a,†}, Xilong Chang^{b,c,†}, Xiaomeng Liang^a, Yan Zhao^d, Guiye Wu^a, Shenghui Xie^a, Pengchen Su^a, Zhiyong Wu^a, Yingang Feng^e, Zhichao Zhang^{a,*}

^a State Key Laboratory of Fine Chemicals, School of Chemistry, Dalian University of Technology, Dalian 116012, People's Republic of China

^b State Key Laboratory of Natural and Biomimetic Drugs, Peking University, Beijing 100191, People's Republic of China

^c Qilu Pharmaceutical Co., Ltd, Shandong 250000, People's Republic of China

^d School of Life Science and Technology, Dalian University of Technology, Dalian 116024, People's Republic of China

^e Qingdao Institute of BioEnergy and Bioprocess Technology, Chinese Academy of Sciences, Qingdao 266101, People's Republic of China

ARTICLE INFO

Article history:

Received 1 September 2012

Revised 28 October 2012

Accepted 8 November 2012

Available online 21 November 2012

Keywords:

Pan-Bcl-2 inhibitor

Bcl-2

Mcl-1

p4 Pocket

Apoptosis

ABSTRACT

Based on the binding mode of our previously discovered dual inhibitor of Bcl-2 and Mcl-1, 3-thiomorpholin-8-oxo-8*H*-acenaphtho[1,2-*b*]pyrrole-9-carbonitrile (**3**, **S1**), a library of 9-substituted **3** derivatives was synthesized to further probe the p4 pocket of the two targets. By NMR, structure–activity relationship study, and site-directed mutation, compound **6d** (3-(4-aminophenylthio)-8-oxo-8*H*-acenaphtho[1,2-*b*]pyrrole-9-3-phenyl)propylamine) was identified to span p2–p4 pockets of Mcl-1, Bcl-2 and Bcl- x_L , and then exhibited 9- to 35-fold better affinity to the three targets than **3** (IC_{50} = 10, 20 and 18 nM, respectively), which led to greater activity in induction of apoptosis in multiple cancer cell lines. Different contribution of p4 pocket to binding Bcl-2 and Mcl-1 was also investigated by plotting the potency and the HAC of the derivatives.

© 2012 Elsevier Ltd. All rights reserved.

1. Introduction

Targeting the interface between proteins has huge therapeutic potential, but discovering small molecule drugs that disrupt protein–protein interactions (PPIs) is an enormous challenge.^{1,2} Some notable successes were achieved with the discovery of BH3 mimetics. These molecules modulate the PPIs between anti-apoptotic and pro-apoptotic Bcl-2 members by occupying the BH3 groove shared by the two opposite functional groups and then induce cancer cells apoptosis.^{3,4} Although the BH3 grooves of Bcl-2

and Bcl- x_L are the primary focus for the design of BH3 mimetics,⁵ recent studies have demonstrated that Mcl-1 also plays an important role for cancer cell survival. It is necessary to neutralize both arms of the anti-apoptotic Bcl-2 family (Bcl-2/Bcl- x_L and Mcl-1) for apoptosis to occur in many cell types.^{6,7} The most potent dual inhibitor (Bcl-2 and Bcl- x_L) ABT-737, for example, is encountering resistance due to the inability to bind a more divergent BH3 groove of Mcl-1 protein.^{8,9} As such, a promising drug-like BH3 mimetic should be a ‘pan-Bcl-2 inhibitor’ that can bind at least Bcl-2 and Mcl-1.³

We have previously reported the discovery of a small-molecule Bcl-2 inhibitor, 3-thiomorpholin-8-oxo-8*H*-acenaphtho[1,2-*b*]pyrrole-9-carbonitrile (**3**, **S1**).^{10–12} The in vivo apoptosis induction by **3** places it on the list of 19 preclinical Bcl-2 inhibitor antitumor drugs.³ Further studies have described the biological mechanism of **3** as an authentic BH3 mimetic and a dual inhibitor that targets both Bcl-2 and Mcl-1.¹¹ In this study, the binding site of **3** was further confirmed by NMR and expanded to that of Bcl- x_L . Although the pan-Bcl-2 inhibition of **3** shows advantages over ABT-737, its affinity toward Bcl-2 (K_i = 310 nM by fluorescence polarization assay (FPA)) is much less potent than ABT-737 (1 nM).⁸ ABT-737 is a highly optimized ligand spanning the p2, p3 and p4 pockets which are sub-active sites in the BH3 groove. According to the X-ray structure of the Bim BH3 peptide in

Abbreviations: Bcl-2, B-cell lymphoma 2; Mcl-1, myeloid cell leukemia sequence 1; Bcl- x_L , B-cell lymphoma x long; Bax, Bcl-2-associated x protein; Bak, Bcl-2 homologous antagonist/killer; BH3, Bcl-2 homology domain 3; SAR, Structure–activity relationship; FPA, fluorescence polarization assay; IC_{50} , the half maximal inhibitory concentration; K_d , dissociation constant; HPLC, high-performance liquid chromatography; ADT, AutoDock tools; ITC, isothermal titration calorimetry; NMR, nuclear magnetic resonance; ELISA, enzyme-linked immunosorbent assay; CCSP, combined chemical shift perturbation; ΔG , binding free energy; HAC, heavy atom count; PDB, protein data bank.

[☆] The 3D structures of human Mcl-1 (PDB ID: 2NLA), Mcl-1 in complex with Bim (PDB ID: 2PQK) and Bcl-2 (PDB ID: 1GJH) were obtained from the protein bank in the RCSB.

* Corresponding author. Tel./fax: +86 411 84986032.

E-mail address: zc Zhang@dlut.edu.cn (Z. Zhang).

[†] These authors contributed equally to this work.

complex with the Bcl-x_L, Bcl-2, and Mcl-1 proteins, four conserved hydrophobic residues (h1–h4) on one face of Bim helix insert into four hydrophobic pockets (p1–p4) within the BH3 grooves of all the three proteins.¹³ The p1–p4 pockets are 4 sub-active hotspots for the structure based design of BH3 mimetics.¹⁴ By SAR studies, our compound **3** may span p2 and p3 but lose p4 pocket.¹²

Here, we designed series of derivatives based on the binding mode of **3** which was further identified by NMR binding study in the present work. We maintained the p2 occupying and expanded to the p4. Many efforts were given to fit both Bcl-2 and Mcl-1 to maintain the dual inhibition. We discovered a new potent pan-Bcl-2 inhibitor 3-(4-aminophenylthio)-8-oxo-8H-acenaphtho[1,2-b]pyrrole-9-(3-phenyl)propylamine (**6d**), which the IC₅₀ value to Mcl-1, Bcl-2 and Bcl-x_L by ELISA was 10, 20 and 18 nM, respectively. The 9- to 35-fold better affinity was achieved for the three targets than its parent **3**. Additionally, we defined the molecular determinants governing the specificity of ligand binding to the p4 pocket of Bcl-2 and Mcl-1.

2. Results and discussion

2.1. Rationale

We recently identified small-molecule **3** as an authentic BH3 mimetic and a dual inhibitor of Bcl-2 and Mcl-1. Herein, we included Bcl-x_L in competitive binding test and found that **3** had similar binding affinities toward Bcl-x_L with Bcl-2 (IC₅₀ = 625 and 710 nM, respectively by ELISA assay) (Table 2 and Table S1). The broader binding profile confirmed **3** as a pan-Bcl-2 inhibitor. Because the three-dimensional structure of Bcl-2 is very similar with that of Bcl-x_L but different with Mcl-1, we continuously focused on BH3 grooves of Bcl-2 and Mcl-1 for lead optimization.

SAR study determined that the carbonyl substitution of **3** binds near R263 of Mcl-1 and the homology of Bcl-2 termed R146 through hydrogen bonds. Its 3-position substituent extends into the p2 pocket, whereas the 9-position cyano group points to but does not access the p4 pocket of the two proteins (Fig. S1).¹² To further identify the binding mode, here we performed a [¹⁵N, ¹H] NMR titration study. In good agreement with the SAR results, the NMR spectra confirmed that **3** occupied the p2 and p3 pocket. The spectra of Mcl-1 alone (shown in blue) showed well-dispersed peaks, indicative of a folded and stable protein. Upon **3** addition, NMR spectra generated many chemical shifts (shown in red), which are indicative of tight binding (Fig. S2a). The combined chemical shift perturbation (CCSP) signals revealed that more than 60% of the residues perturbed above 0.02 ppm were located in the BH3 binding groove of the protein (Fig. 1a). Among them, some residues located in p2 and p3 pockets (V253, M250, R263, L246, F270 and K234) experience average chemical shift changes of at least 0.04 ppm (Fig. 1c). There were several residues that experienced intensity reductions associated with line broadening. In particular, R263 and the nearing V253 had large intensity changes following the addition of **3**, to a point where they were no longer detectable (Fig. S2b). It supported the formation of the hydrogen bond in this area.

With the aim of accessing the p4 pocket to achieve enhanced dual inhibition effects, we designed series of **3** derivatives that the cyano group was replaced by longer and larger groups. Previous studies have reported that Bcl-2 and Mcl-1 show differences in the structure of their p4 pockets.¹⁵ When we tried to occupy the p4, an optimization path should be carefully designed to resolve differences of the p4 between Bcl-2 and Mcl-1 without losing either one.

At the outset, we aimed to maintain the binding mode with R263 in Mcl-1 and R146 in Bcl-2 constant since the key hydrogen bond was formed in this region. We then sought to the X-ray structure of the non-selective peptide Bim (BH3) in complex with

Bcl-2-like proteins. The comparison of high-resolution structure study of Bcl-x_L/Bim and Mcl-1/Bim showed that R263 in Mcl-1 is somewhat less solvent-exposed than its homologue in Bcl-x_L.¹⁶ Since Bcl-2 and Bcl-x_L have quite similar structure with overall backbone RMSD (root mean square deviation) only 1.85 Å,¹⁷ we concluded the R263 in Mcl-1 and its homologue in Bcl-2 might render an obvious difference in this region between the two proteins. Consistently, our computational modeling studies illustrated that the R263 of Mcl-1 was less solvent-exposed than R146 of Bcl-2 (Fig. 2a and b). We proposed that if **3** derivatives would like to maintain the binding mode with R263 in Mcl-1 and R146 in Bcl-2, efforts should be given to adapt to the difference. Additionally, a recent molecular dynamics study has reported a greater openness of the p4 binding sites on Mcl-1 than Bcl-2.¹⁵ Given these findings, we inferred that the angle of the BH3 groove of two proteins in the p4 region would be different when a molecule fits into BH3 groove of Mcl-1 and Bcl-2. Bcl-2 could tolerate a relative open angle, whereas a closed angle may be favored by Mcl-1. A previously molecule TM-179 also met our hypothesis. When it bound to Bcl-2, the 2-hydroxyl was used for hydrogen bond with R146. But an alternative 3-hydroxyl was used for corresponding hydrogen bond when bound to Mcl-1.¹⁸ However, **3** contains one hydrogen bond available group. We proposed when the interaction with R263 or R146 was kept, a flexible linker group between the core structure of **3** and the p4-occupying group at 9-position should be chosen for the accommodation by both Bcl-2 and Mcl-1.

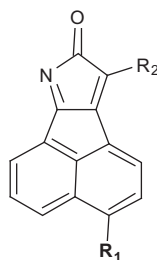
Additionally, because Bim BH3 peptide utilized F69 to occupy p4 pocket, F69 becomes the mimicking goal of newly designed group to occupy p4.¹⁹


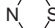

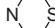

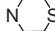
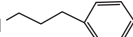
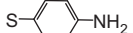
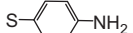

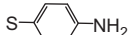

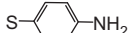
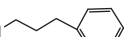
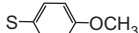
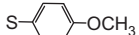

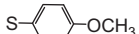

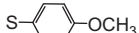
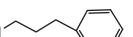
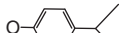
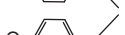

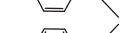

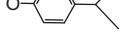

Lastly, the molecular planarity and symmetry of the core of **3** has a general negative impact on solubility. Introduction of additional groups at 9-position would lead to the disruption of molecular planarity and symmetry, which could improve its solubility.²⁰ Thus, optimizing at 9-position of **3** could improve not only its binding potency, but perhaps also its solubility.

2.2. Structure–activity relationship

We initially substituted the cyano with amino as a linker group, which may render flexibility to compounds to allow them engage well into the p4 pocket of both Bcl-2 and Mcl-1. Meanwhile, amino could facilitate solubility by forming hydrogen bond with water. We sought to survey a variety of alkyl group in order to identify those win appropriate trajectory and length to access p4 pocket, meanwhile maintaining dual inhibition. Specifically, we examined ethylamine, *n*-propylamine, *n*-butylamine, *n*-pentylamine, and *n*-hexylamine groups, yielding analogues 3-thiomorpholin-8-oxo-8H-acenaphtho[1,2-*b*]pyrrole-9-ethylamine (**5a**), 3-thiomorpholin-8-oxo-8H-acenaphtho[1,2-*b*]pyrrole-9-*n*-propylamine (**5b**), 3-thiomorpholin-8-oxo-8H-acenaphtho[1,2-*b*]pyrrole-9-*n*-butylamine (**5c**), 3-thiomorpholin-8-oxo-8H-acenaphtho[1,2-*b*]pyrrole-9-*n*-pentylamine (**5d**) and 3-thiomorpholin-8-oxo-8H-acenaphtho[1,2-*b*]pyrrole-9-*n*-hexylamine (**5e**), respectively (Scheme 1). Different with parental **3**, most of the 9-substituted derivatives have interruption to FPA by the autofluorescence. Thus, we took enzyme-linked immunosorbent assay (ELISA) to measure their abilities to competitively displace a Bim-derived peptide from Mcl-1 and Bcl-2, respectively. Triton X-100 was added as a detergent to prevent the possible aggregation of hydrophobic compounds, as described in the supporting information. The competitive binding curves of these compounds to Bcl-2 and Mcl-1 were outlined in Figure 3a and b. R(–)-Gossypol was used as positive control.¹⁴ Compound **3** was tested for comparison. While weaker binding affinity was found for **5a**, better binding affinities than **3** toward Mcl-1 and Bcl-2 were found for **5b–5e**. A progressive increase in length of the substituent (b < c < d < e) resulted in a corresponding increase in Mcl-1 and Bcl-2 affinity. Compound

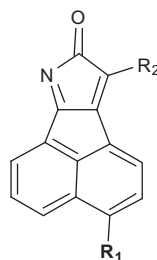
3,9 Substituted **3** derivatives: name, structure, HAC and binding affinity toward Mcl-1 by ELISA (IC₅₀, nM)



Compounds	R ₁	R ₂	HAC	IC ₅₀ (nM)	pK _d	ΔG (kcal mol ⁻¹)
3		CN	24	95	7.02	9.65
5c		HN 	27	79	7.10	9.76
5e		HN 	29	37	7.43	10.21
5h		HN 	32	15	7.82	10.75
6a		CN	26	90	7.04	9.68
6b		HN 	29	50	7.30	10.03
6c		HN 	31	30	7.53	10.34
6d		HN 	34	10	8.00	10.99
7a		CN	27	388	6.41	8.81
7b		HN 	30	150	6.82	9.38
7c		HN 	32	78	7.11	9.77
7d		HN 	35	42	7.38	10.14
8a		CN	28	321	6.49	8.92
8b		HN 	31	141	6.85	9.41
8c		HN 	33	75	7.10	9.75
8d		HN 	36	39	7.41	10.18

Because **5b–5e** were analogues with straight-chain substituent, we tried to replace the linear group with bulkier group to probe the surrounded areas between the arginine residue and p4. As such, we synthesized **5f** and **5g** with isopropyl and benzyl substitution, respectively. By ELISA, we found that **5f** and **5g** completely lost binding affinity to Bcl-2 ($>10\ \mu\text{M}$), indicative of steric clashes in Bcl-2 protein. However, **5f** retained a weak binding affinity to Mcl-1 ($2.5\ \mu\text{M}$) and **5g** showed a sub-micromolar affinity ($521\ \text{nM}$). The different selectivity by these two compounds raised a possibility that the surrounded area at this position of Bcl-2 is different from that at Mcl-1. We calculated the width of this area by AutoDock tools, and found that the Bcl-2 R146 and Y108 residues narrowed the area by $8\ \text{\AA}$, compared to the corresponding Mcl-1 R263 and H224 residues, which was $14.4\ \text{\AA}$ (Fig. S3). As such, Bcl-2 could not accommodate **5f** and **5g** with bulkier group. As for Mcl-1, it could accommodate the more conformationally restrained benzyl (**5g**) substitution but cannot accept the steric bulky isopropyl (**5f**) substitution. It was further confirmed by docking

We also explored the effect of rigid group on the dual inhibition by substituting the cyano with ester as the linker group. As expected, the conversion of amino group to a rigid ester negatively impacted the potency. Ethoxycarbonyl and *n*-propoxycarbonyl substitution yielded compounds **4a** and **4b** (Scheme 1) showed dramatically decreased affinities than **5c** and **5d**. No binding affinities to Mcl-1 (>10 μ M) and very weak affinities to Bcl-2 (2.2 and 2.1 μ M, respectively) were found for them. It is reasonable to attribute the loss of affinity to the rigid C–O–C=O, which formed a dihedral equal to 0° or 180°²¹ These results suggested a flexible linker are favorable for binding the two protein targets.

Table 23,9 Substituted **3** derivatives: name, structure, HAC and binding affinity toward Bcl-2 by ELISA (IC₅₀, nM)

Compounds	R ₁	R ₂	HAC	IC ₅₀ (nM)	pK _d	ΔG (kcal mol ⁻¹)
3		CN	24	715	6.15	8.44
5c		HN	27	198	6.70	9.21
5e		HN	29	96	7.02	9.64
5h		HN	32	49	7.31	10.04
6a		CN	26	331	6.48	8.90
6b		HN	29	190	6.72	9.23
6c		HN	31	80	7.10	9.75
6d		HN	34	20	7.70	10.58
7a		CN	27	945	6.02	8.28
7b		HN	30	356	6.45	8.86
7c		HN	32	206	6.69	9.19
7d		HN	35	57	7.24	9.95
8a		CN	28	739	6.12	8.42
8b		HN	31	322	6.49	8.92
8c		HN	33	184	6.74	9.25
8d		HN	36	42	7.38	10.14

Having optimized the linker with flexible and linear character, we now tried to utilize a benzene group to mimic the F69 of non-selective peptide Bim for occupying p4 pocket. Since **5b**, **5c**, **5d** and **5e** have accessed p4 pocket, we added benzene to the terminus of the alkyl chain of these compounds, yielding 3-thiomorpholin-8-oxo-8H-acenaphtho[1,2-b]pyrrole-9-(3-phenyl)propylamine (**5h**), 3-thiomorpholin-8-oxo-8H-acenaphtho[1,2-b]pyrrole-9-(3-phenyl)butylamine (**5i**), 3-thiomorpholin-8-oxo-8H-acenaphtho[1,2-b]pyrrole-9-(3-phenyl)pentylamine (**5j**) and 3-thiomorpholin-8-oxo-8H-acenaphtho[1,2-b]pyrrole-9-(3-phenyl)hexylamine (**5k**). In ELISA assay, **5h** exhibited the most potent binding affinity to Bcl-2 (49 nM) and Mcl-1 (15 nM), which achieved nearly 12- and 6-fold better affinities toward Bcl-2 and Mcl-1, respectively than **5b**. Compound **5i** also showed about 2- to 3-fold improved affinities than **5c**. However, **5j** exhibited a significant decrease of binding affinities to Bcl-2 (1.3 μM) and Mcl-1 (1.1 μM) compared to **5d**. Compound **5k** showed a similar loss of affinity. In agreement with it, docking results of **5h** and **5j** showed that 3-phenylpropyl was properly located in the p4 pocket of Mcl-1, while the 3-phenylpentyl of **5j** was repulsed out by the p4 pocket (Fig. 4c and d). Therefore, an alkyl group with three carbons was the optimal length to mimic the northern part of D67 to F69 of Bim peptide.

In our previous SAR study, aminophenylthio group at the 3-position was identified to fit p2 better than thiomorpholin. Methoxyphenylthio and isopropylphenoxy were groups that could fit p2 but not as well as thiomorpholin.¹² In order to discover more potent inhibitors by spanning p2 and p4, and gain insights into the druggability of the p2 and p4 pockets, we selected 3-(4-aminophenylthio)-8-oxo-8H-acenaphtho[1,2-b]pyrrole-9-carbonitrile (**6a**), 3-(4-methoxyphenylthio)-8-oxo-8H-acenaphtho[1,2-b]pyrrole-9-carbonitrile (**7a**) and 3-(4-isopropylphenoxy)-8-oxo-8H-acenaphtho[1,2-b]pyrrole-9-carbonitrile (**8a**) as starting compounds for further optimization at 9 position. Series **6** (**6a–6d**), **7** (**7a–7d**), and **8** (**8a–8d**) were synthesized (Table 1). We found that butyl, hexyl and 3-phenylpropyl substitution brought about a corresponding increase of binding affinity to Bcl-2 and Mcl-1 in the three series (Tables 1 and 2), which was in agreement with the results of **5c**, **5e** and **5h**. Comparably, the rank order of binding affinities for certain 9-substituted analogues from series **5**, **6**, **7** and **8** was keeping the same as the rank order of p2-occupying efficiency, which is **6a** > **3** > **8a** > **7a**. We also tested the binding affinities of **3** derivatives toward Bcl-x_L and gained the same trend of improvement (Table S1). Among them, the most potent **6d** displayed IC₅₀ values of 10, 20 and 18 nM for Mcl-1, Bcl-2 and Bcl-x_L, respectively, which is 9–35 times more effective than **3**.

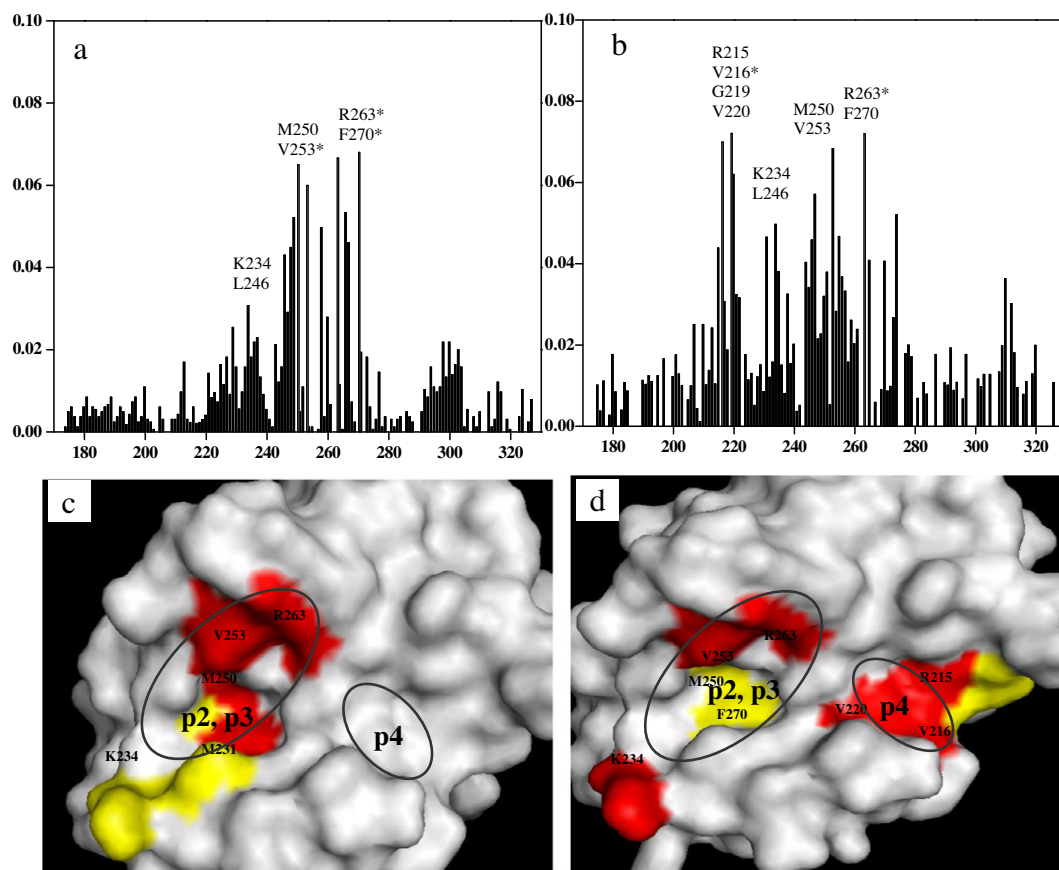


Figure 1. Amide proton and nitrogen CCSP of Mcl-1 derived from the ^1H - ^{15}N HSQC spectra after titration with (a) **3** to Mcl-1 and (b) **6b** to Mcl-1. Resonances that disappeared upon binding are shown as gray bars. That was V253, R263 and F270 for **3**, and V216 and R263 for **6b**. (c, d) Chemical shift perturbations of residues induced by **3** and **6b** mapped onto the structure of Mcl-1. The Mcl-1 residues showing chemical shift changes of $0.03 < \Delta\text{CS} < 0.06$ were colored yellow, and residues showing with $\Delta\text{CS} > 0.06$ or for which the cross-peaks disappeared upon binding were colored red.

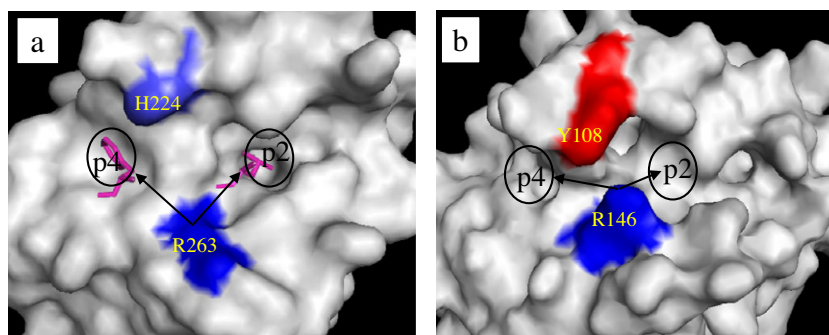


Figure 2. Surface depiction of the three-dimensional structures of (a) Mcl-1 (PDB: 2PQK) and (b) Bcl-2 (PDB: 1GJH). The p2 and p4 interacting residues L62 and F69 in Bim complex with Mcl-1 were shown in pink, respectively. Different angles of the BH3 groove of two proteins in the p4 region were shown with arrows.

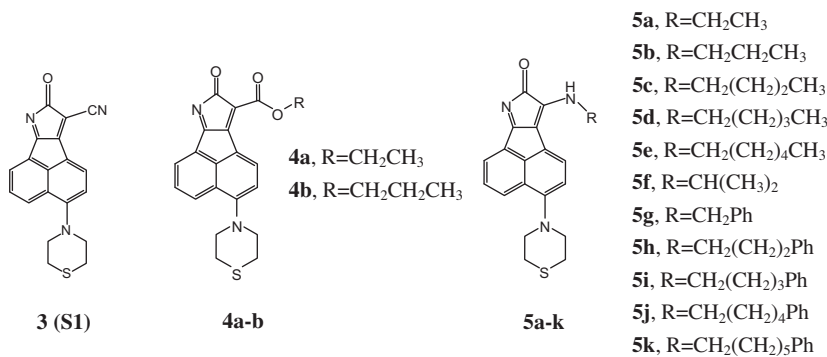
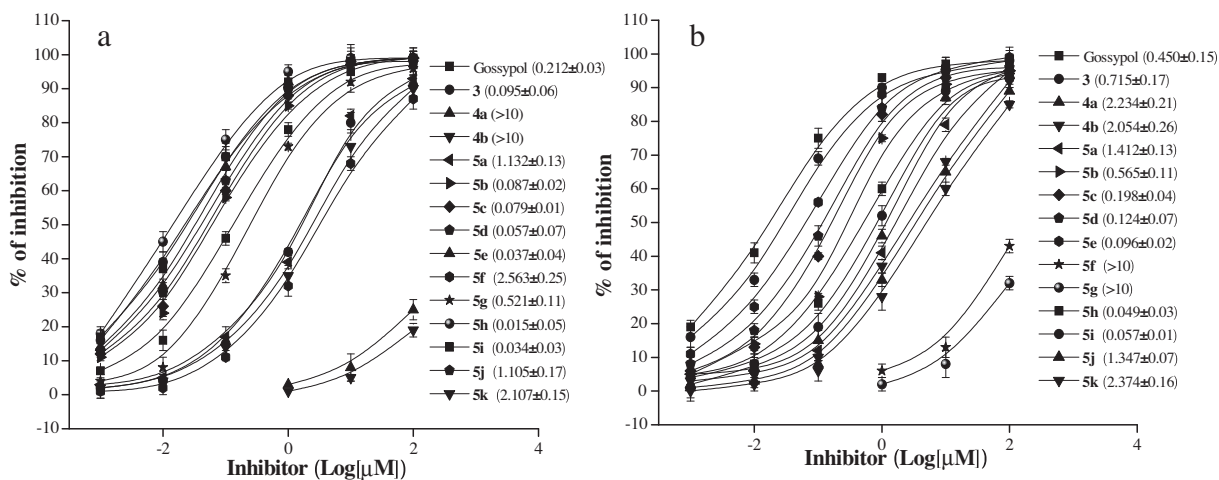
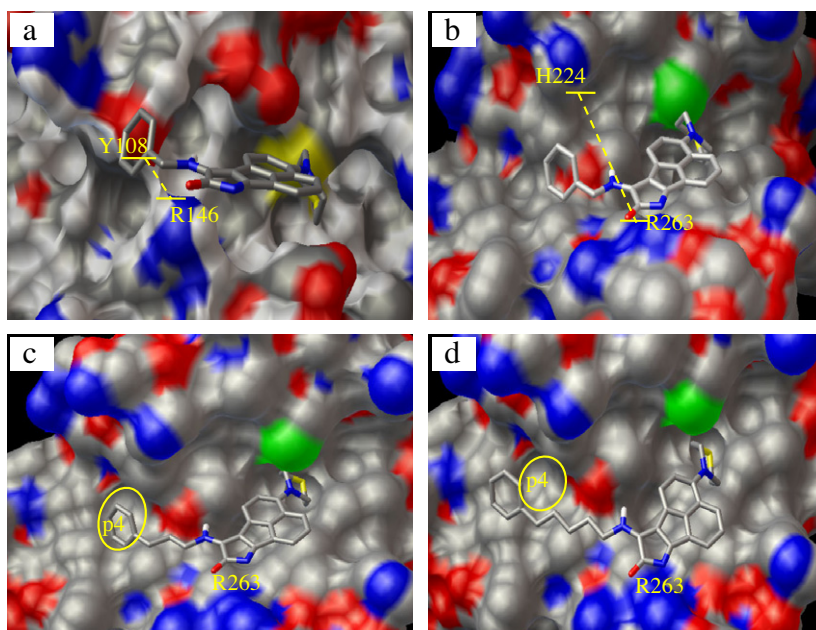
To confirm the results of the ELISA assay data, we also performed isothermal titration calorimetry (ITC) assay with **6d** and **3** in parallel. In consistent with the improvement in IC_{50} values, **6d** exhibited a K_d value of 105 nM, which was about ninefold improved than that of **3** ($K_d = 964$ nM, Fig. 5).

2.3. Identification of binding site by site-directed mutagenesis and NMR

R263 of Mcl-1 and the R146 of Bcl-2 have been determined to form a hydrogen bond with carbonyl of **3**. To examine whether R263 still played an important role in the binding of newly designed **3**, 9 substituted **3** derivatives, we constructed a

site-directed mutant on R263A and evaluated the binding affinities of some representative analogues toward wild-type Mcl-1 and Mcl-1 R263A mutant, respectively by using ITC. **6d**, for example, showed a 20-fold lower affinity toward R263A mutant (2.34 μM , Table 3 and Fig. S4) than wild-type Mcl-1. The similar decrease was found for other compounds (Table 3). It supported that R263 still served as an anchor residue by forming hydrogen bond network with **3**, 9 substituted **3** derivatives. Together with the same rank order of p2-occupying efficiency, we proposed that these derivatives gained increased affinity by additional occupation of p4 pocket when maintained the p2 occupation.

To further determine the binding site, we produced uniformly ^{15}N -labeled Mcl-1 protein and performed NMR titration by **6b**,

Scheme 1. Structures of **3**, **4a–b**, and **5a–k**.Figure 3. Competitive binding curves of (–)-Gossypol, **3**, **4a–b**, **5a–k** to (a) Mcl-1 and (b) Bcl-2 as determined by ELISA assay.Figure 4. Predicted binding model of **5g** in complex with (a) Bcl-2, (b) Mcl-1, (c) **5h** in complex with Mcl-1, and (d) **5j** with Mcl-1. The carbon, oxygen, nitrogen atoms were shown in gray, red and blue. The sulfur atom was shown in yellow and green for Bcl-2 and Mcl-1, respectively.

because **6b** is more soluble than **6d** in Mcl-1 solution. We measured two-dimensional [¹⁵N, ¹H] NMR spectra in the absence

and presence of **6b**, respectively. Figure S2c showed an overlay of the spectra before (blue) and after (red) the addition of **6b**,

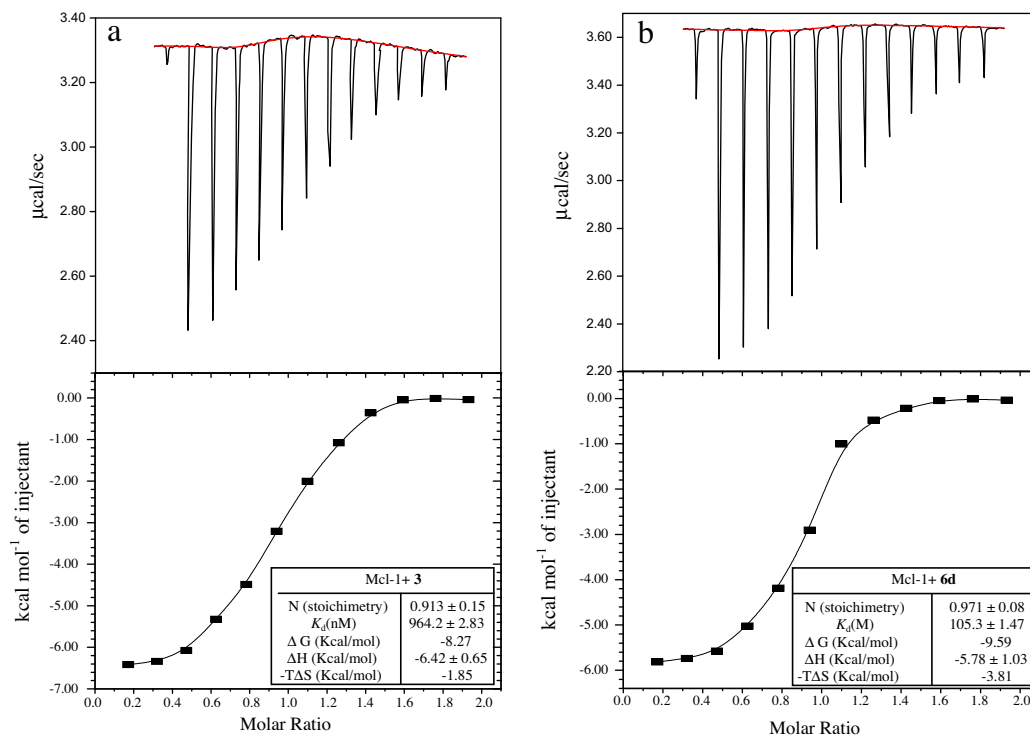


Figure 5. (a) Raw data for titration of **3** and (b) **6d** into Mcl-1. Titrations consisted of $12 \times 3 \mu\text{L}$ injections of compound at $300 \mu\text{M}$ into Mcl-1 ($30 \mu\text{M}$). Each peak corresponds to one injection. K_d value was calculated from integration of the raw data.

together with close-up views of selected residues that underwent large chemical shift changes in the presence of **6b** (Fig. S2d). Figure 1b showed a plot of the chemical shift perturbations against the overall Mcl-1 protein residues. Above 60% residues affected by the binding of **6b** were located in the BH3-binding pocket of Mcl-1, indicating that **6b** binds in the BH3-binding groove of Mcl-1. When compared with NMR spectra for **3** (Fig. 1a), a same cluster of residues in p2 including R263, V253, L246, M250, F270 and K234 experienced average chemical shift changes of at least 0.05 ppm (Fig. 1b). Notably, another cluster of residues including V220, R215, V216 and G219 which experienced at changes of at least 0.06 ppm emerged after adding **6b**. In particular, R263 and V216 are no longer detectable. Mapping these residues into 3D structure of Mcl-1 showed their locations within and surrounding the p2 and p4 pocket (Fig. 1d). So far, we identified that **6b** occupied p2 and p4 simultaneously.

2.4. Comparing the different contribution of p4 to binding affinity between Bcl-2 and Mcl-1

The alanine scanning studies have shown when F69 of Bim was mutated to alanine, it lost most of the affinity to Bcl-x_L. However the mutant can still bind Mcl-1 in the same range even it lost p4 occupation.²² Additionally, a broader p4 pocket in Mcl-1 than that in Bcl-2 has been revealed by a molecular dynamics study.¹⁵ These studies suggested that the p4 pocket has less contribution to Mcl-1 binding. In the present study, however, we found binding affinities to Mcl-1 were progressively improved accompanied with increased p4 occupation. We inferred that p4 occupying was still a dominant contributor for a molecule to bind to Mcl-1. Notably, for an optimized compound, it was improved less dramatically for Mcl-1 (average eightfold) than for Bcl-2 (average 17-fold), such as compound **5h**, **6d**, **7d**, and **8d**. It suggested the contribution of p4 was different between the two proteins.

To further illustrate the contribution of p4 occupation to Bcl-2 and Mcl-1, respectively, we calculated the contribution of

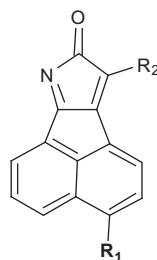
p4-occupying groups per atom by plotting the potency against the HAC in serials **5**, **6**, **7**, and **8**. When a certain 3-position substituent was chosen to occupy p2, groups with an increased size were substituted at 9-position to occupy p4. As shown in Figure 6a for Mcl-1, a linear relationship between potency and HAC was found for compounds **3**, **5c**, **5e** and **5h**. When plotted with the other serials, nearly parallel trend lines were found, with an average value for the slope of $0.16 \text{ kcal mol}^{-1}$ per heavy atom. These data implied that the parental core remained unchanged and that the 9-position substituent was simply added the p4 occupation. Given the constancy of slope in different serials, the same binding efficiency of 0.16 should be directly related to the contribution of p4 in Mcl-1. As for Bcl-2, co-linear relationships between potency and HAC were also found in the four serials. However, the average value for the slope was approximately $0.21 \text{ kcal mol}^{-1}$ per heavy atom. It suggested that additional groups to occupy p4 contributed less affinity to Mcl-1 than Bcl-2. From the aspect of p4 pocket, the binding site of Bcl-2 might be more druggable than that of Mcl-1.

2.5. Improved solubility of 3, 9 substituted 3 derivatives

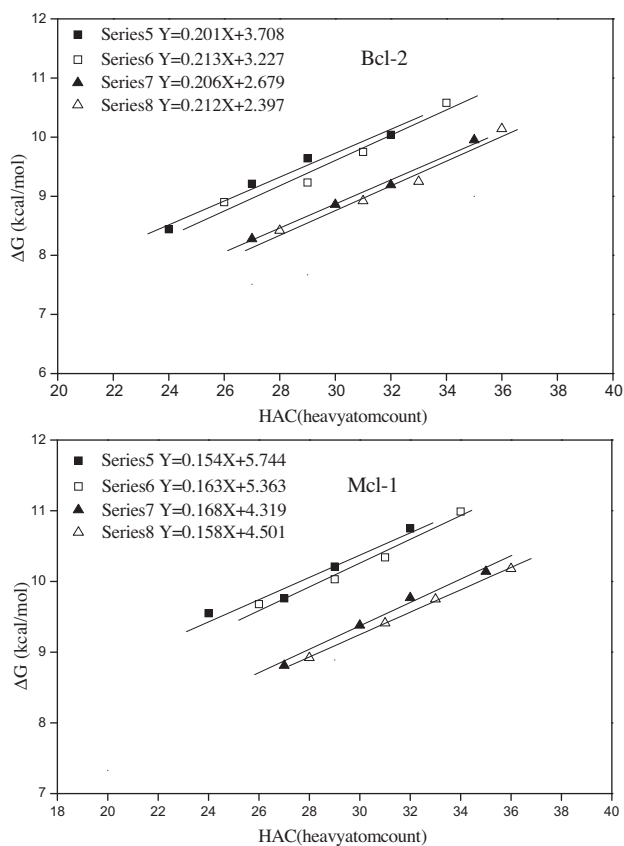
Next, we tested the solubility of **3**, **6b** and **6d** in 1% DMSO/H₂O which has been accepted to be orally and intravenously available for drug treatment in vivo.²³ As shown in Tables 4 and 3 was practically insoluble (0.002 mg/mL) in this solvent, while the solubility of **6b** and **6d** could reach 0.027 and 0.018 mg/mL, respectively. The increase of solubility showed the improved drug-like properties compared to **3**.

2.6. 3,9 Substituted 3 derivatives induce apoptosis by binding to the BH3 groove of Bcl-2 and Mcl-1

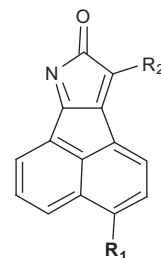
We next determined whether the improved binding affinities of **6b** and **6d** toward both Bcl-2 and Mcl-1 could translate into greater disruption of Bcl-2/Bax and Mcl-1/Bak complexes in living cells. We applied multiple cell lines with different levels of Mcl-1 and

Table 3Binding affinity of compounds with Mcl-1 and R263A mutant by ITC Assay (K_d , μM)

Compound	R ₁	R ₂	Mcl-1 (wild-type)	Mcl-1 (R263A)
R-(–)-Gossypol	—	—	2.324	—
3		CN	0.954	28.73
6b			0.512	12.75
6d			0.105	2.34
8c			0.802	19.15

**Figure 6.** Free energy of binding (in kcal mol^{-1}) for compounds of series **5**, **6**, **7** and **8** plotted as a function of the number of heavy atoms in the ligands. See Table 1.

Bcl-2, that is, human chronic myelogenous leukemia cell line K562, myeloid leukemia cell line HL-60 and breast cancer cell line MCF-7. Among them, K562 and HL-60 express the highest level of Mcl-1 and Bcl-2, respectively (Fig. 7a). By co-immunoprecipitation (Co-IP) assays, we found that **6b** and **6d** exhibited greater potential than **3** to disrupt Bcl-2/Bax and Mcl-1/Bak complexes. Meanwhile,

Table 4Solubility of **3**, **6b** and **6d** in 1% DMSO/H₂O (mg/mL)

Compound	R ₁	R ₂	1%DMSO/H ₂ O (mg/mL)
3		CN	0.002
6b			0.027
6d			0.018

the compounds released cytochrome c to cytosome in the same order as the complexes disruption (Fig. 7b and c). These data demonstrated that **6b** and **6d** exhibited enhanced apoptosis induction than **3** through disrupting complexes of Bcl-2 and Mcl-1.

Compound **3** has been identified as a pure BH3 mimetic that kills via Bax/Bak completely. Most of the recently developed nanomolar inhibitors (six of seven) such as Gossypol (BL-193, AT-101) are not pure BH3 mimetics and then showed unexpected toxicity.^{8,24} Next, we determined whether or not **6b** and **6d** retained the property of **3** as a pure BH3 mimetic. Bax and Bak was both silenced in MCF-7 cells by shRNA (Fig. S5). Gossypol was used as a negative control. After 12 h of exposure to 5 μM of compounds, cytochrome c release was examined. In contrast with cytochrome c release in wild-type MCF-7 cells, no cytochrome c release was found for **3**, **6b** and **6d** in Bax- and Bak-deleted cells. However, the same amount of cytochrome c release as that in wild-type cells was detected for Gossypol (Fig. 7d and e). This strongly supported that **6b** and **6d** killed completely dependent on Bax/Bak. The pure

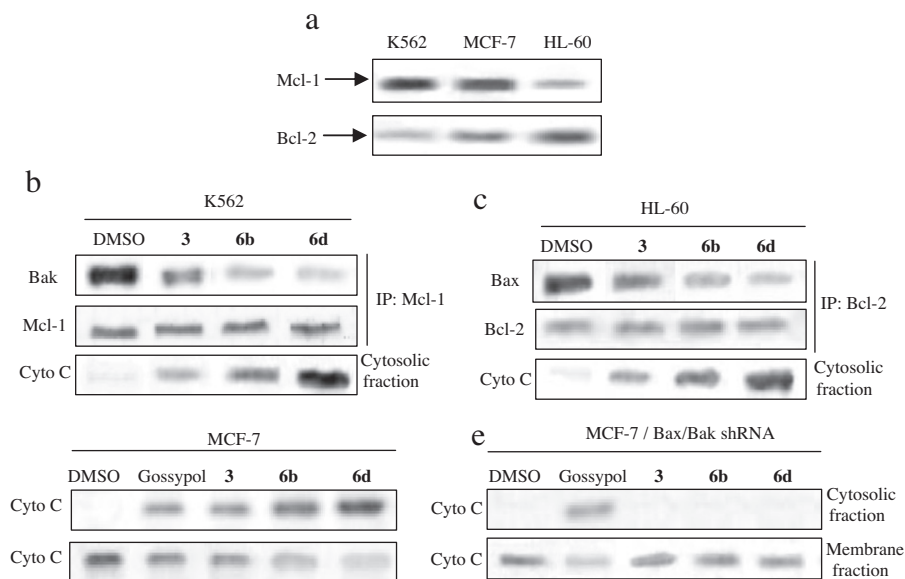


Figure 7. (a) The levels of Mcl-1 and Bcl-2 protein in K562, MCF-7 and HL-60 cells were examined by Western blot. (b) K562 and (c) HL-60 cells were treated with 5 μ M **3**, **6b**, **6c** or **6d** for 12 h. Harvested cells were subjected to immunoprecipitation of Mcl-1 and Bcl-2 followed by western blot analysis for Bak and Bax, respectively. The paralleled harvested cells were lysed in digitonin lysis buffer. After centrifugation, the supernatant (S-100, cytosolic fraction) were collected and subjected to western blot for cytochrome c. (d) Wild-type MCF-7 cells and (e) Bax/Bak shRNA transfected cells were treated with 5 μ M indicated compounds, respectively, followed by cytochrome c detection in S-100 fraction.

BH3 mimicking property of these derivatives could render them an attractive aspect in the future clinical development.

3. Conclusions

We substituted the 9-position of **3** to probe the different p4 pockets in Bcl-2 and Mcl-1. [^{15}N , ^1H] NMR, SAR studies and site-directed mutation determined that when the key interaction with R263 in Mcl-1 and its homologue in Bcl-2 was maintained constant, flexible amino liker made derivatives accepted by the different angle of the BH3 groove of two proteins in the p4 region. Additionally, a broader space between R263 and p4 of Mcl-1 than that of Bcl-2 was identified by small molecules. Ultimately, the most potent compound **6d** that contained a three-carbon alkyl group to optimally mimic the northern part of D67 to F69 of Bim peptide and utilized the terminal benzene to mimic F69, exhibited 9- to 35-fold improvement than **3** with IC_{50} values of 10, 20 and 18 nM toward Mcl-1, Bcl-2 and Bcl-x_L, respectively. Excitingly, its improved binding affinity also translated to greater potency of disrupting Bcl-2/Bax and Mcl-1/Bak complex in cells, resulting in enhanced apoptosis induction in multiple cancer cell lines with variant Mcl-1 and Bcl-2 expression levels. Together with pure BH3 mimicking property and improved solubility than **3**, **6b** and **6d** represent novel potent lead drugs for cancer therapy.

In addition, we showed co-linear relationships of potency against the HAC by 9-position substituted derivatives with the slope of 0.16 and 0.21 kcal mol^{-1} per heavy atom for Mcl-1 and Bcl-2, respectively. It suggested that p4 occupying could contribute to dual Bcl-2 and Mcl-1 inhibitor, but the contribution was less for Mcl-1 than Bcl-2.

4. Experimental

4.1. Chemistry

The synthesis of **6b** and **6d** is shown in [Supplementary data Scheme 3](#). **6b**. Yield: 23%. ^1H NMR (400 M, CDCl_3): δ 8.74 (br, 1H), 8.57 (d, $J = 8.0$ Hz, 1H), 8.47 (d, $J = 8.0$ Hz, 1H), 8.44 (d,

$J = 8.0$ Hz, 1H), 7.88 (t, $J = 8.0$ Hz, 1H), 7.63 (d, $J = 8.0$ Hz, 2H), 7.56 (d, $J = 8.0$ Hz, 1H), 7.38 (d, $J = 8.0$ Hz, 2H), 3.89 (m, 2H, $-\text{NHCH}_2\text{CH}_2-$), 3.45 (br, 2H), 1.75 (m, 2H, $-\text{NHCH}_2\text{CH}_2\text{CH}_2-$), 1.41 (m, 2H, $-\text{CH}_2\text{CH}_2\text{CH}_2\text{CH}_3$), 0.94 (t, $J = 8.0$ Hz, 3H). TOF MS (EI^+): $\text{C}_{24}\text{H}_{21}\text{N}_3\text{OS}$, (m/z): calcd for 399.0401, found 399.0405. HPLC system 1: purity = 99.03%, $t_R = 15.7$ min. HPLC system 2: purity = 99.29%, $t_R = 5.16$ min.

Compound **6d**. Yield: 19%. ^1H NMR (400 M, CDCl_3): δ 8.57 (d, $J = 8.0$ Hz, 1H), 8.47 (d, $J = 8.0$ Hz, 1H), 8.44 (d, $J = 8.0$ Hz, 1H), 7.88 (t, $J = 8.0$ Hz, 1H), 7.63 (m, 4H), 7.56 (d, $J = 8.0$ Hz, 1H), 7.47 (m, 3H), 7.38 (d, $J = 8.0$ Hz, 2H), δ 6.74 (br, 1H), 3.89 (m, 2H, $-\text{NHCH}_2\text{CH}_2-$), 3.55 (br, 2H), 1.75 (m, $-\text{NHCH}_2\text{CH}_2\text{CH}_2-$, 2H), 1.41 (m, 2H, $-\text{CH}_2\text{CH}_2\text{CH}_2\text{Ph}$). TOF MS (EI^+): $\text{C}_{29}\text{H}_{23}\text{N}_3\text{OS}$, (m/z): calcd for 461.0588, found 461.0585. HPLC system 1: purity = 98.73%, $t_R = 17.56$ min. HPLC system 2: purity = 99.29%, $t_R = 4.06$ min.

4.2. ELISA assay

An enzyme-linked immunosorbent assay was reported as previous. For this assay, Biotinylated Bim peptide (residues 81–106, biotin-(β)A-(β)A-D-M-R-P-E-I-W-I-A-Q-E-L-R-R-I-G-D-E-F-N-A-Y-Y-A-R-R-amide, hereafter called biotin-Bim) was diluted to 0.09 $\mu\text{g/mL}$ in SuperBlock blocking buffer in PBS (Pierce Biotechnology, Inc, Rockford, IL, catalog # 37515) and incubated for 1.5 h in 96-well microtiter plates already coated with streptavidin (Qiagen, Catalog # 15500) to allow the formation of the complex between Biotin-Bim and streptavidin. All incubations were performed at room temperature unless otherwise noted. Each inhibitor was first dissolved in pure DMSO to obtain a 10 mM stock solution. Next, serial dilutions of compounds with 0.01% Triton X-100 were incubated with 20 nM protein in PBS for 1 h. The plates were washed three times with PBS containing 0.05% Tween-20. The inhibitor and protein mixture (100 μL) were transferred to the plate containing the biotin-Bim/streptavidin complex and incubated for 2 h. The plate was then washed as before and mouse anti-His antibody that conjugated with horseradish peroxidase (Qiagen, Catalog # 34460) was added into the wells and incubated for 1 h. The plate was then washed with PBS containing 0.05%

Tween-20. Finally, TMB (100 μ L, Beyotime, Catalog # P0209) was added to each well; the enzymatic reaction was stopped after 30 min by addition of H_2SO_4 (100 μ L, 2 M). Absorbances were measured with a TECAN GENios (Swiss, TECAN) microplate reader using a wavelength of 450 nm. Three independent experiments were performed with each inhibitor to calculate average IC_{50} value and standard deviation (SD).

4.3. ITC assay

Isothermal titration calorimetry (ITC) was performed using iTC200 (Microcal). Experiments were performed in 20 mM Tris pH 8.0, 150 mM NaCl, 1% DMSO at 25 $^{\circ}\text{C}$. For evaluating K_d value of **6d** compared with that of **4**, titrations consisted of $12 \times 3 \mu\text{L}$ injections of compound at 300 μM into Mcl-1 (30 μM). For evaluating K_d values of analogues toward wild-type Mcl-1 compared with that toward Mcl-1 R263A, titrations consisted of $16 \times 2.5 \mu\text{L}$ injections of compound at 500 μM into Mcl-1 (50 μM). All sample data obtained after control data corrections were analyzed to fit to a one-site model. For control ITC experiments, the sample cells were filled with assay buffer and the compound solution was added. This process was identical to that for protein samples.

4.4. NMR spectroscopy

^{15}N , ^1H HSQC spectra were recorded for 0.1 mM ^{15}N -labeled Mcl-1. Compound **3** and **6b** stock solution was added at a 4:1 ratio, respectively. The $^1\text{H}/^{15}\text{N}$ HSQC spectra were recorded on a Bruker Advance DRX600 MHz spectrometer, processed by NMRPipe and visualized by NmrViewJ 8.0. Chemical shift changes were calculated as $((\Delta^1\text{H ppm})^2 + (0.2 \times \Delta^{15}\text{N ppm})^2)^{0.5}$ as a function of the residue number.

Acknowledgments

The authors would like to thank Professor Zhongjun Li (State Key Laboratory of Natural and Biomimetic Drugs, Peking University, Beijing, People's Republic of China) for the discussion. The work was partly supported by the Fundamental Research Funds for the Central Universities (DUT11SM08) and partly supported by the National Natural Science Foundation of China (81273436).

Supplementary data

Supplementary data associated with this article can be found, in the online version, at <http://dx.doi.org/10.1016/j.bmc.2012.11.008>.

References and notes

- Sackett, D. L.; Sept, D. *Nat. Chem.* **2009**, *1*, 596.
- Veselovsky, A. V.; Archakov, A. I. *Curr. Comput. Aided Drug Des.* **2007**, *3*, 51.
- Azmi, A. S.; Mohammad, R. M. *J. Cell. Physiol.* **2009**, *218*, 13.
- Zhang, L.; Ming, L.; Yu, J. *Drug Resist. Updates* **2007**, *10*, 207.
- Vogler, M.; Dinsdale, D.; Dyer, M. J.; Cohen, G. M. *Cell Death Differ.* **2009**, *16*, 360.
- Warr, M. R.; Shore, G. C. *Curr. Mol. Med.* **2008**, *8*, 138.
- Bednarek, J.; Wesierska, J. D.; Kilianska, Z. M. *Postepy Biochem.* **2007**, *53*, 228.
- Delft, M. F. V.; Wei, A. H.; Mason, K. D.; Vandenberg, C. J.; Chen, L.; Czabotar, P. E.; Willis, S. N.; Scott, C. L.; Day, C. L.; Cory, S.; Adams, J. M.; Roberts, A. W.; Huang, D. C. *Cancer Cell* **2006**, *10*, 389.
- Konopleva, M.; Contractor, R.; Tsao, T.; Samudio, I.; Ruvolo, P. P.; Kitada, S.; Deng, X.; Zhai, D.; Shi, Y. X.; Sneed, T., et al. *Cancer Cell* **2006**, *10*, 375.
- Zhang, Z. C.; Jin, L. J.; Qian, X. H.; Wei, M. J.; Wang, Y. Y.; Wang, J. *ChemBioChem* **2007**, *8*, 113.
- Zhang, Z. C.; Song, T.; Zhang, T. T.; Gao, J.; Wu, G. Y.; An, L. J. *Int. J. Cancer* **2010**, *128*, 1724.
- Zhang, Z. C.; Wu, G. Y.; Xie, F. B.; Song, T.; Chang, X. L. *J. Med. Chem.* **2011**, *54*, 1101.
- Lee, E. F.; Czabotar, P. E.; Smith, B. J.; Deshayes, K.; Zobel, K.; Colman, P. M.; Fairlie, W. D. *Cell Death Differ.* **2007**, *14*, 1711.
- Wang, G.; Nikolovska-Coleska, Z.; Yang, C. Y.; Wang, R.; Tang, G.; Guo, J.; Shanqary, S.; Qiu, S.; Gao, W.; Yang, D., et al. *J. Med. Chem.* **2006**, *49*, 6139.
- Acoca, S.; Cui, Q.; Shore, G. C.; Purisima, E. O. *Proteins* **2011**, *79*, 2624.
- Czabotar, P. E.; Lee, E. F.; Van Delft, M. F.; Day, C.; Smith, B. J.; Huang, D. C. S. *Proc. Natl. Acad. Sci. U.S.A.* **2007**, *104*, 6217.
- Bruncko, M.; Oost, T. K.; Belli, B. A.; Ding, H.; Joseph, M. K.; Kunzer, A.; Martineau, D.; McClellan, W. J.; Mitten, M.; Nq, S. C., et al. *J. Med. Chem.* **2007**, *50*, 641.
- Tang, G.; Nikolovska-Coleska, Z.; Qiu, S.; Yang, C. Y.; Guo, J.; Wang, S. J. *Med. Chem.* **2008**, *51*, 717.
- Fire, E.; Gulla, S. V.; Grant, R. A.; Keating, A. E. *Protein Sci.* **2010**, *19*, 507.
- Ballard, P.; Bradbury, R. H.; Harris, C. S.; Hennequin, L. F.; Dickinson, M.; Kettle, J. G.; Kendrew, J.; Klinowska, T.; Ogilvie, D. J.; Pearson, S. E.; Williams, E. J.; Wilson, I. *Bioorg. Med. Chem. Lett.* **2006**, *16*, 4908.
- Lopes, S.; Lapinski, L.; Fausto, R. *Phys. Chem. Chem. Phys.* **2002**, *4*, 5952.
- Lee, E. F.; Czabotar, P. E.; Delft, M. F.; Michalak, E. M.; Boyle, M. J.; Willis, S. N.; Puthalakath, H.; Bouillet, P.; Colman, P. M.; Huang, D. C.; Fairlie, W. D. *J. Cell Biol.* **2008**, *180*, 341.
- Mui, E. J.; Schiehsler, G. A.; Milhous, W. K.; Hsu, H.; Roberts, C. W.; Kirisits, M.; Muench, S.; Rice, D.; Dubey, J. P.; Fowble, J. W., et al. *PLoS Negl. Trop. Dis.* **2008**, *2*, e190.
- Lei, X.; Chen, Y.; Du, G.; Yu, W.; Wang, X.; Qu, H.; Xia, B.; He, H.; Mao, J.; Zong, W., et al. *FASEB J.* **2006**, *20*, 2147.